Development of a Model for the Small-Particle Orbital Debris Population Based on the STS Impact Record

J. Seago[1], M. Matney[2], A. Vavrin[3]

[1]ERC – Jacobs JETS Contract, NASA Johnson Space Center, Mail Code XI5-9E,
2101 NASA Parkway, Houston, TX 77058, USA, john.h.seago@nasa.gov
[2]NASA Johnson Space Center, Mail Code XI5-9E, 2101 NASA Parkway, Houston, TX 77058, USA
[3]GeoControl Systems – Jacobs JETS Contract, NASA Johnson Space Center, Mail Code XI5-9E,
2101 NASA Parkway, Houston, TX 77058, USA

ABSTRACT

In preparation for the release of the Orbital Debris Engineering Model (ORDEM) version 3.1, the NASA Orbital Debris Program Office (ODPO) revisited how orbiting debris populations of characteristic sizes smaller than 1 cm were modeled. The primary contributor to the population of sub-centimeter debris particles is the surface deterioration or erosion of spacecraft materials exposed to the outer-space environment. Because small particulates are not directly trackable by remote sensing, the primary means of detection is via historical counts of small impact features on flown radiator and window surfaces of the U.S. Space Transportation System (STS, also known as the Space Shuttle) from 1995-2011. Historic NASA studies of high-velocity impact tests have related impact-feature size to particle mass and velocity for certain STS surfaces, so that a corresponding particle size may be inferred from each small-impact feature observed. Micro-debris populations are then estimated by modeling the path and orientation of an STS mission through a simulated debris environment, and the densities of this simulated environment are rescaled to approximate the number of observed STS impact features. Monte-Carlo methods are further employed to gauge the estimation uncertainty of the rescaled environment. A description of the chosen methodologies for estimating and adjusting the micro-debris population model, and the results, are presented.

1   DEBRIS-FLUX COMPUTATION

ORDEM is an engineering model that describes the orbital-debris environment from 10 μm and 10 m in terms of yearly binned orbital elements distributions, broken out by particle size and material density within the LEO and GEO regions. To assess risk to spacecraft, ORDEM relies on computed flux: the directional rate per unit time for debris from a specific population of particles larger than a certain size threshold that would strike an idealized spherical satellite with unit cross-sectional area ($\pi r^2 = 1$ m^2). The flux on a spacecraft is computed using the concept of an encompassing 3-dimensional "igloo" around the spacecraft, where each "igloo" element is defined as a finite element in elevation (or pitch), azimuth (or yaw), and relative velocity spaces. The spacecraft's orbit (perigee altitude, eccentricity, and inclination) is used to calculate this "igloo" map of directional fluxes as a function of debris size, material type, and relative velocity in the spacecraft frame. The flux on specific surfaces of a spacecraft is computed by using the areas and unit normal of these surfaces relative to the "igloo" element directions. For a given spacecraft orbit, there exists a unique mapping between any directional "igloo" element and any debris orbit distribution element. Once the mapping matrix is computed, then any orbit distribution file (sorted by year, size, and material density) can be used to compute the flux in each "igloo" element [1].

The spacecraft flux is integrated over an entire orbit, calculating the fraction of the orbital period spent at different points in its orbit, and requiring the spatial density and velocity vector of each component sub-population at those points. The spatial density for the LEO micro-debris populations is computed by assuming that the arguments of perigee and ascending nodes of orbits for debris source-object are from a uniformly random distribution. Random assignments of the argument of perigee and ascending node varies the directionality and relative velocities within the population, which can be used to map the population uncertainties into flux uncertainties. For most LEO debris, this assumption is reasonable, although there are certain orbital regimes where the assumption of thoroughly randomized nodal distribution does not strictly hold until the long term, such as frozen orbits (*e.g.*, sun-synchronous and *Molniya*), and debris from recent fragmentation events.

2   OBSERVATIONAL DATA

The primary means of micro-debris detection is via historical counts of small impact features on returned surfaces. NASA's Hyper Velocity Impact Technology (HVIT) group maintains a database of impact-feature measurements on STS surfaces (Fig. 1), based on post-flight surveys by NASA personnel at Johnson Space Center (JSC) and Kennedy Space Center [2]. Impact-crater residues were assessed at NASA JSC by Scanning Electron Microscopy-Electron Dispersive X-ray (SEM-EDX) to estimate the elemental composition and mass densities of impactors, and to distinguish which features are from orbital micro-debris impacts. Constituents were classified as being of low density (LD; $\rho < 2$ g/cm^3), medium density (MD; $2 \leq \rho \leq 4.5$ g/cm^3), or high density (HD; $\rho > 4.5$ g/cm^3). However, due to the small number of low-density debris impactors identified, LD constituents were grouped together with MD objects. This resulted in ORDEM 3.1 development using two density classes: MD ($\rho \leq 4.5$ g/cm^3) and HD. To establish realistic micro-debris populations for ORDEM 3.1, the count of impacts to STS radiators and windows from 1995–2011 (STS 71 through STS 133) were used to re-scale the initial modeled degradation populations that were based on an assumed particle-production rate. These STS impact datasets were the same as those used for building ORDEM 3.0 but were reanalyzed for use in ORDEM 3.1.
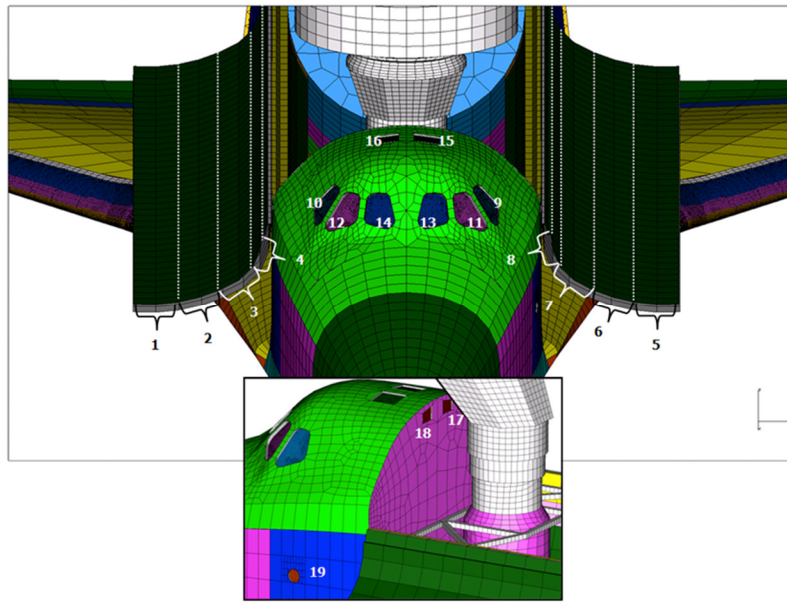

Fig. 1. Surveyed STS surfaces (window and radiator) used for ORDEM 3.1,
each surface facing a specific direction with a specific field of regard.

2.1   STS Windows

Nine STS crew-module windows were used for modeling the micro-debris environment. This relatively small surface area (3.4 m^2 total) revealed most of the impacts recorded in the impact dataset, because the polished outer thermal panes allowed for the detection of very small impact features. The residues of many materials, including aluminum alloys, were reliably detected on the fused-silica outer thermal panes because the substrate does not contain these elements. The nominal in-flight STS orientation made the aft-facing cargo-bay windows (17 and 18 in Fig. 1) far less susceptible to orbital debris impacts, so these were excluded in the degradation model development.

Table 1. OD window impacts (323) by residue material types.

Material	%	Density	Material	%	Density
Plastic	0.6	*LD*	Steel	12.4	HD
Aluminum	39.6	MD	Titanium	4.3	HD
Paint	39.6	MD	Copper	0.6	HD
Aluminum Oxide	4.3	MD	Silver	0.6	HD

A total of 86 STS flights were examined post-flight in window surveys, recording 1986 total impact features within the HVIT database. Categorization of window impact-feature residues resulted in approximately 70% (1398) classified as indeterminate ("unknown", UN); 13% (265) as micrometeoroids (MM); and 16% (323) as orbital micro-debris (OD). For window craters identified as originating from orbital-debris impacts, SEM-EDX analysis suggested the constituent breakdown in Table 1. During ORDEM 3.1 development, the window impacts from "unknown" impactors were randomly assigned as belonging to either the MM or OD categories, using rounded percentages of "known" MM and OD measured on the windows: MM 45%, MD OD 46%, and HD OD 9%.

2.2 STS Radiators

Eight radiator panels mounted on the inside surface of the STS payload doors offered a total surface area of approximately 119 m^2, a relatively large surface area (7.6% of vehicle total) that increased the number and size of expected impact features. The radiators were fabricated with an aluminum thermal facesheet, and were covered with silver-Teflon thermal-control tape. Three types of damage were typically recorded: holes in the thermal tape, craters in the facesheet, and perforations of the facesheet. Sixty-seven STS missions were examined post-flight in radiator surveys, recording 133 facesheet tape holes, 436 facesheet craters, and 81 facesheet perforations (holes). SEM-EDX categorization of radiator impact residues resulted in approximately 70% (450) unknown; 13% (86) MM; and 16% (104) OD, an outcome proportionally identical to the window distribution. Concerns existed about the accuracy of thermal-tape hole measurements, as well as the completeness of surveys for the non-perforating radiator craters due to their small sizes. Because radiator perforations were the most critical damage to repair between missions, this population was characterized most completely. Therefore, ORDEM 3.1 development only considered the dataset of complete perforations. Radiator penetration features were categorized as 26% (21) unknown; 26% (21) MM; and 48% (39) OD. The constituent breakdown from SEM-EDX analysis, limited to radiator penetration features from OD, is provided in Table 2. Aluminum is not evident in Table 2, as aluminum residues cannot be readily identified against the radiator's aluminum substrate. When all 21 of the unknowns were treated as aluminum impactors (MD), the ratio of MD-to-HD was still lower than that of the windows, supporting the assumption that most of the perforations by unknown particles were likely caused by aluminum impactors.

Table 2. OD radiator penetration features (39) by residue material type.

Material	%	Density	Material	%	Density
Paint	41.0	MD	Titanium	5.1	HD
PC Board	5.1	MD	Brass	2.6	HD
Steel	43.6	HD	Lead	2.6	HD

2.3 Impactor-Size Estimation (Damage Equations)

Impactor sizes from *in-situ* impact data must be inferred from the feature sizes. Extensive hypervelocity impact range testing by HVIT has yielded sufficient data to develop so-called damage equations – empirical relationships that convert projectile properties and impact circumstances (diameter d_p, mass density ρ, relative impact velocity v, and impact angle relative to the surface normal θ) to impact characteristics such as crater depth, crater diameter, or perforation diameter. Their general form is:

$$Y = c \cdot d_p^\alpha \cdot \rho^\beta \cdot v^\gamma \cdot (\cos\theta)^\delta, \tag{1}$$

where the coefficients $\{c, \alpha, \beta, \gamma, \delta\}$ are estimated from laboratory samples of observed impact feature characteristics (Y), such as crater depth, crater diameter, or perforation diameter. Window crater depth, P_{depth} (cm) is related to the characteristic length of the impactor, or impactor diameter d_p (cm), as [3]:

$$P_{depth} = 0.530 \cdot d_p^{1.06} \cdot \rho^{0.5} \cdot (v \cdot \cos\theta)^{\frac{2}{3}}, \tag{2}$$

where ρ is mass density (g/cm^3), v is the relative impact velocity (km/s), and θ is the relative impact angle. Similarly, window crater diameter D (cm) is related to impactor diameter d_p (cm) by:

$$D = 30.9 \cdot d_p^{1.33} \cdot \rho^{0.44} \cdot (v \cdot \cos\theta)^{0.44}. \tag{3}$$

The equation for the diameter of a radiator facesheet perforation D_{fs} (mm) as a function of the impactor diameter d_p (mm) is given by:

$$D_{fs} = 0.611 \cdot d_p^{0.957} \cdot \rho^{0.231} \cdot v^{0.638} \cdot (cos\ \theta)^{-0.145} \ . \tag{4}$$

Another damage equation also exists to estimate the transition from a closed crater to full perforation. Analyses indicated that the perforation size estimate D_{fs} did not work well for the case where a particle *barely* perforates. Consequently, the particle-size estimate from perforation diameter was considered accurate only if the measured perforation $D_{fs} \geq 1$ mm. However, it was possible to use the smaller perforation data by employing a ballistic limit equation that estimates whether any perforation will occur, given the particle diameter and approach velocity:

$$d_p = 1.05 \cdot \rho^{-\frac{1}{3}} \cdot (v \cdot cos\ \theta)^{-\frac{2}{3}} \ . \tag{5}$$

Equations 2 through 4 can be inverted to solve for an unknown characteristic length, or impactor diameter d_p, if the impact velocity and angle are (assumed) known. Estimates of d_p maintained by the HVIT impact database assume a 45° impact angle and a relative velocity of 23 km/s for micrometeoroids and a mission-specific or altitude-specific average relative velocity for orbital debris. Because a smaller impactor traveling rapidly can create a similar feature as a larger impactor traveling slowly, a population distribution of d_p can be estimated via simulation by sampling distributions of impact parameters such as impact angle and velocity. ORDEM 3.1 development used a probabilistic analysis of environment and orbiter vehicle surface pointing direction to determine distributions in d_p as a function of distributions in relative velocity and impact angle. Approximately, the window impacts sample the 10 μm – 300 μm size debris environment, and radiator perforations sample the 300 μm – 1 mm range.
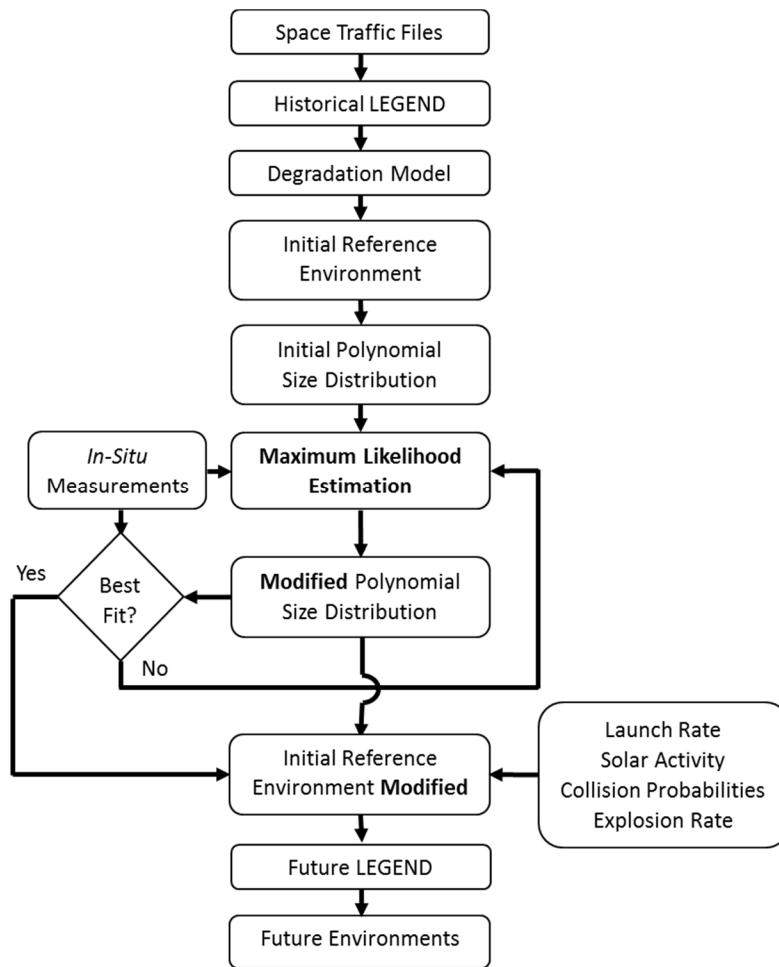

Fig. 2. Process flow of the small particle (10 μm to 3.16 mm) estimation methodology.

3   DEGRADATION MODEL DEVELOPMENT

The degradation model simulates production of micro-debris particles and provides the reference populations for the micro-debris population for particle sizes from 10 μm to 1 mm. For certain materials such as paint, exposure to the atomic oxygen environment and thermal cycling may be the primary mechanism [4]. For metallic particles, ejecta from micro-debris impacts and micrometeoroid impacts may be an important contributor. The physics of the degradation process is not yet fully understood; consequently, simulated micro-debris were created based on a constant rate of resident space-object surface erosion. The initial number of particulates created by a surface degradation process was assumed to be proportional to the surface area of each contributing source. The initial size-dependent production rates of micro-debris were then adjusted to be compatible with observational data (Section 2). Fig. 2 illustrates the process flow of degradation model development.

3.1   Micro-Debris Source Modeling

Micro-debris source objects greater than 10 cm (rocket bodies, spacecraft, and mission-related debris) contributing to the initial reference "background" populations were simulated using NASA's evolutionary LEO-to-GEO ENvironment Debris model LEGEND [5]. Software input files maintained by the ODPO ("Space Traffic Files", Fig. 2) contain information on known historical populations, such as resident objects, maneuvers in space, and fragmentation events. However, intact source objects with perigee altitude greater than 5000 km, or apogee altitude less than 500 km, were omitted. Micro-debris from high-altitude source objects would not be expected to penetrate the LEO environment within the projected lifetime of the model, and micro-debris from very low-altitude source objects have negligibly short lifetimes. Omitting source objects below 500 km also discounted temporal contributions from human spaceflight activity. The orbits of the small debris created by the model were binned by orbit parameters and the orbit population densities. Historical simulation spanned from 1957 to 2015 and emulated known historical space traffic deterministically using a semi-analytical orbital theory, with decayed objects removed from the environment. To simulate future traffic ("Future LEGEND", Fig. 2), future populations were added via an 8-year launch cycle, with 90% rate of compliance with post-mission disposal (PMD) guidelines assumed for spacecraft and rocket bodies. Historical and future breakup clouds were modeled using the NASA Standard Satellite Breakup Model [6] for sizes 1 mm and larger.

3.2   Micro-Debris Initial Reference Environment

A medium density subpopulation (ρ = 2.8 g/cm^3) and a high-density subpopulation (ρ = 7.9 g/cm^3) were spawned simultaneously from orbiting source objects based on an initial production rate of 0.1 particles/m^2/month (particles pairs per surface area per time interval), the time interval on orbit, and the assumed surface area of each orbiting source object ("Degradation Model", Fig. 2). Each number of simulated MD/HD micro-debris particles were calculated from random draws of a Poisson distribution based on the initial production rate. These particles initially shared the same orbit as their source body (zero relative velocity), but their orbits evolved from each other over time due to solar-pressure and atmospheric-drag perturbations, driven by the differences in the area-to-mass ratios between the particles and their parent source.
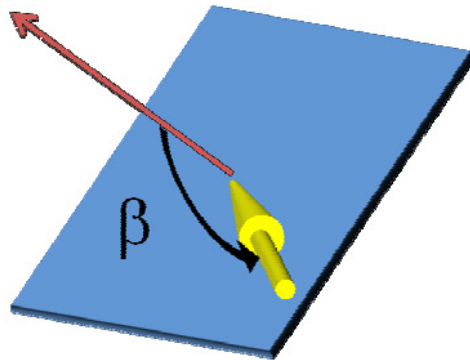

Fig. 3. Inbound-flux direction β measured relative to the normal of the local surface horizontal.

3.3   Area-Time Products (MARK Files)

Using the HVIT impact database, the attitudes of the as-flown STS surfaces (window and radiator) were modeled to incorporate the directionality of the debris flux for each surface and mission. This detailed accounting includes the masking of surfaces by other spacecraft components, such as when the Shuttle was docked to the International Space Station (ISS). The area-time products for each exposed surface and each Shuttle mission were saved in so-called "MARK files" generated by the HVIT group [7]. The threat directions of the debris environment (defined as the direction from which an inbound flux in the local horizontal plane will arrive at the surface, Fig. 3) are mapped to the angle of impact relative to the surface normal; this mapping is in the form of a matrix and maintained in a file specific to each surface. The area-time products were calculated using 90 equally-spaced threat directions in the spacecraft local horizontal plane. The angles relative to the surface normal were divided into nine 10° segments. The number tabulated represents the area-time product for an STS surface, with the projection area for off-normal impacts already taken into account. The calculation of the presented area of specific surfaces was an intermediate step in mapping the predicted degradation production rates to the STS impact data.

4   MODELING PROCEDURE

The general procedure for using *in-situ* measurement data for ORDEM 3.1 required the following: determining which missions should be included for each analysis, assigning impact features to material density categories, and defining the sizing and range of application of feature-sizes. Careful analysis of the data per mission suggested that the window impact measurements were not complete to the same minimum size; therefore, measurements below a mission-specific limiting size threshold were ignored (Section 2.1).

To specify the model parameters in terms of the reference model populations, simulated MD and HD particles were assigned to one of 50 size bins distributed logarithmically from 10 μm to 3.16 mm. Using the orbit of each STS mission, the size-dependent spacecraft flux "igloo" was computed from the reference populations, using the MARK files to predict the velocity and direction-dependent flux for each surface, and predicting the corresponding feature size distributions, logarithmically binned from 10 μm to 10 mm.
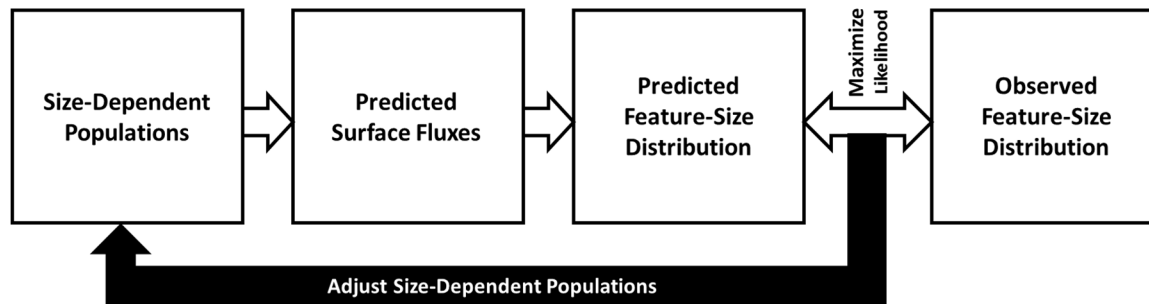

Fig. 4. Schematic for comparing modeled surface flux with observed feature-size distribution.

4.1   Fitting Procedure

Fig. 4 outlines the general process of comparing the modeled fluxes on a surface with the corresponding observed feature-size distribution for the same surface. The initial background populations predicted the modeled flux on each STS surface for each mission, and damage equations (Section 2.3) related the modeled flux as a function of size, velocity, and direction to a predicted feature-size distribution. This method becomes straightforward as the distribution of size, velocity, and direction flux in the spacecraft frame are all predicted by the model, and the mapping of these flux distributions to each surface is provided by the MARK files (Section 3.3), which accounts for the detailed pointing histories for each surface for each mission. For ORDEM 3.0 development, flux was combined over all missions and adjustments were made based on the combined impact counts from the total window area and total radiator area. Fluxes partitioned by mission and surface increased the fidelity of ORDEM 3.1 model fits by preserving the directionality of the surfaces at the different mission altitudes. Double arrows in Fig. 4 indicate where comparisons between the (observed) model and the (computed) data were made in the process, to estimate a size-dependent scale estimate to be applied to the initial background populations.

4.2 Method of Maximum Likelihood

Maximum Likelihood Estimation (MLE) was employed by comparing the computed Poisson expectation for each feature size bin, each surface, and each mission against the measured number of features seen. Specifically, if a feature-size bin j has d_j features, and the Poisson-predicted feature count for bin j is m_j, then the likelihood that the observed number of features d_j are a sample from the model is:

$$\wp = \prod_j \frac{e^{-m_j}(m_j)^{d_j}}{d_j!}. \tag{6}$$

$\wp$ is the multiplicative product of the Poisson probabilities from each (independent) size bin; however, it is computationally easier to maximize the natural logarithm of the likelihood, so that Equation 6 becomes a sum:

$$\mathcal{L} = \sum_j \{-m_j + d_j \ln(m_j) - \ln(d_j!)\}. \tag{7}$$

The MLE algorithm systematically adjusts the modeled parameters used to compute the predicted counts (m_j) until Equation 7 reaches a maximum value. For ORDEM 3.1, a multi-dimensional simplex method [8] was used to solve for the parameters of two separate fitting functions representing the MD and HD scale factors across the 50 micro-debris size categories. These fitting functions were parameterized as continuous 3rd-order log-log polynomials, which were evaluated at the values of the 50 half-decadal size categories. The solutions were iterated until the method converged on a best-fit solution (the log-likelihood was maximized). Because multidimensional searches can sometimes converge to local maxima, restarting techniques were employed to better isolate global maxima.

The resulting fits were examined and compared to different subsets of the data, such as low-altitude (< 450 km) and high-altitude (> 450 km) missions. Statistical tests verified that the data were a reasonable sample of the fitting functions. Limiting the number of estimated parameters was also important; using too many polynomial terms resulted in highly oscillatory behavior, whereas using too few did not fit the data well. For ORDEM 3.0, a similar estimation process was employed with 5th-order polynomials, but an additional constraint was applied to the distribution curve at larger sizes, where observations are sparse. However, ORDEM 3.1 used a lower-order fit without a terminal constraint at large particle sizes to permit larger variation and provide more stability in the results of the Monte-Carlo trials (used to estimate flux uncertainties, Section 4.3), and thus was likely to be more indicative of the actual uncertainty. The lower order on the polynomial also smoothed out wild variations in the curve that were introduced for some of the Parametric Bootstrap resample cases.

4.3 Population Means and Uncertainties

The micro-debris population uncertainty was estimated via Monte Carlo methods using four primary steps:

1. The observational data counts were prepared by randomly reassigning unknown impacts, proportionate to known impacts of MD, HD, and micrometeoroids (MM) for windows (Section 2.1). For radiator perforations, all unknowns remained assigned to MD (Section 2.2).
2. With unknowns having been reassigned from Step 1, the newly resampled observational data (d_j) were used to re-estimate size-dependent scale factors (modeled as two log-log cubic polynomials, see Section 4.2) for the MD and HD sub-populations using the MLE algorithm.
3. A parametric bootstrap procedure [9] was applied to the fitted MD and HD scale-factor functions. The re-estimated scale factors and basis populations from Step 2 were used to compute the predicted number of features in each feature size bin. These new "data" (simulated d_j) were sampled by using these predictions as the expectation value for a Poisson sampler. These Poisson draws model a random sample from such a distribution.
4. Like Step 2, new scale factors were again re-estimated using the MLE, with the newly simulated observational data counts from Step 3 used as the observational data d_j.

The four steps were repeated $N = 10000$ times to create a large sample of population scale-factor estimates from which a sample mean and variance was computed to provide a measure of the size-dependent uncertainty in the estimated model parameters. The advantage of this process is that it accounts for uncertainty due to the random assignment of unknown impacts (Step 1) and estimation uncertainty from the choice of model. The square root of the sample variance (s) models the population uncertainty as a function of sample size according to:

$$s = \sqrt{\frac{1}{N-1}\sum_{i=1}^{N}(x_i - \bar{x})^2},$$

(8)

where x_i is a scaling estimate for the ith estimate based on simulated data and $\bar{x}$ is the arithmetic mean of x_i.

5   RESULTS

Comparisons between the model and data are shown in Fig. 5 and Fig. 6 for the ISS and Hubble Space Telescope (HST) mission-altitude regions respectively; the radiator facesheet perforations were converted to distributions in particle size using the inverse of Equation 4 and Equation 5 to verify ORDEM 3.1 fluxes, and to compare with
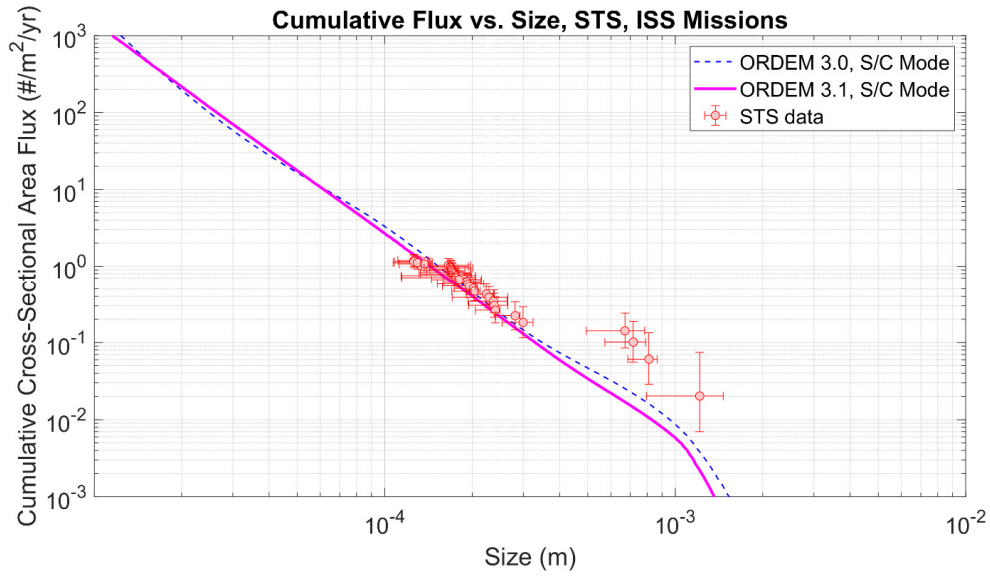

Fig. 5. Cumulative cross-sectional area flux (spacecraft mode) vs. size for ORDEM 3.0, ORDEM 3.1, and STS radiator perforation data from ISS missions.
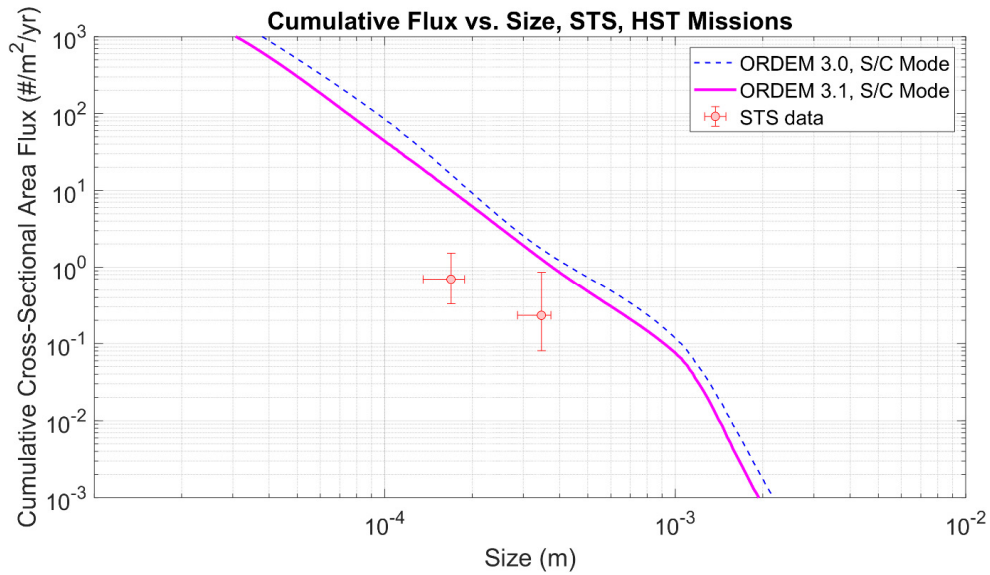

Fig. 6. Cumulative cross-sectional area flux (spacecraft mode) vs. size for ORDEM 3.0, ORDEM 3.1, and STS radiator perforation data from Hubble Space Telescope missions.

ORDEM 3.0. Horizontal uncertainties represent the asymmetric 68th-percentile (1 σ) uncertainties from the distribution obtained in d_p and implies a measure of confidence in the particle-size determination given the observed perforation diameter. Cumulative counts were converted into cumulative cross-sectional area flux by dividing the impact count by the aggregated presented-area-time product over the total duration of the applicable missions. Vertical uncertainties represent the 68th-percentile uncertainties in the cross-sectional area flux computed from the Poisson probability model from reported counts.
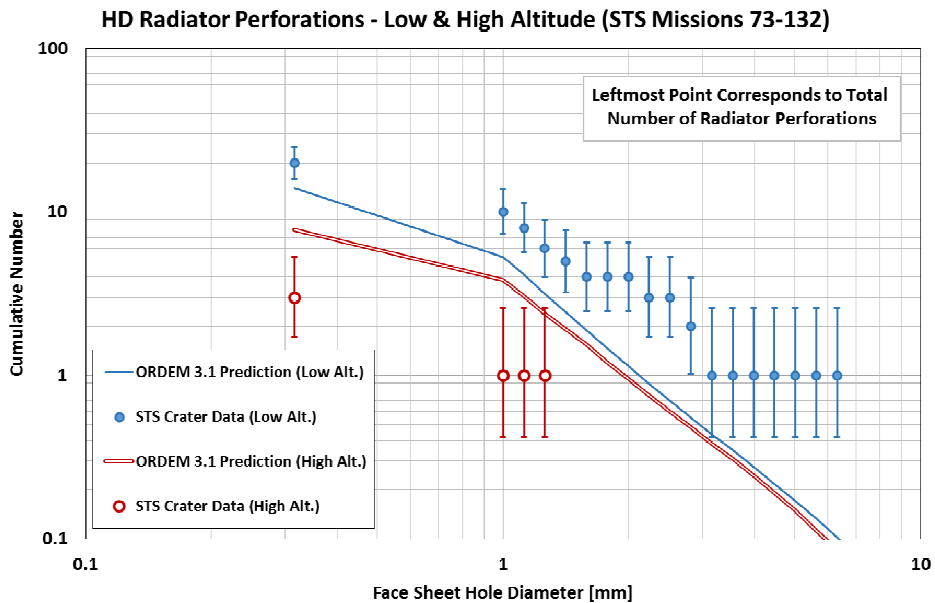

Fig. 7. Cumulative number of STS HD radiator perforations vs. ORDEM 3.1 predicted facesheet perforation diameter, with HD STS impact data by low- and high-altitude missions. The data are within the 95% confidence limit of the distribution. The model "splits the difference" between low-altitude and high-altitude HD observations. Note that the low-altitude prediction would match the data better if the single, large rightmost point did not exist.
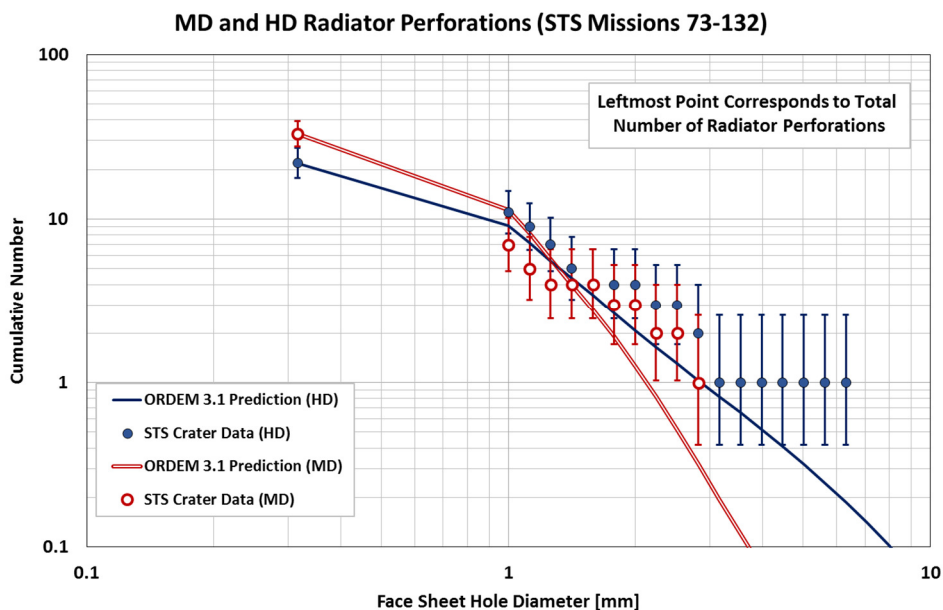

Fig. 8. Cumulative number of radiator perforations vs. facesheet perforation diameter for ORDEM 3.1 predictions, with MD and HD STS impact data from all missions. The data confidence limit is within 90% of the distribution.

Fig. 5 shows a generally good agreement between ORDEM 3.1 and the flux determined from the STS radiator facesheet perforations, particularly for the smaller sizes where more counts are available. The comparison at higher altitudes (STS servicing missions to the HST) shown in Fig. 6 is not quite as good, but there were also significantly fewer impacts from those post-mission surveys. Because the model was scaled to best fit the radiator-perforation data, the model performs better at lower altitudes where there were more observations. Fig. 7 and Fig. 8 show the comparison between the measured cumulative number of radiator facesheet perforations as a function of size, and the distribution predicted by ORDEM 3.1 from the final degradation population. The ORDEM flux was multiplied by the aggregated presented-area-time product to represent expected accumulated count on the STS radiators. The isolated point on the left of Fig. 7 is the predicted and measured total number of perforations of any size using Equation 5. The statistical tests used to evaluate quality of fit involved Monte-Carlo Poisson sampling from the model distributions and the computation of the log-likelihood from each sample. The confidence limit was computed by comparing the log-likelihood of the actual data with the distribution of log-likelihoods from the Monte Carlo sampled data. If the observation-data log-likelihood was higher than at least 10% of the sampled distribution, then it was deemed to be within the 90% confidence limits.

6   CONCLUDING REMARKS

For ORDEM 3.1 development, sources of micro-debris (≤ 3 mm) were scaled based on *in-situ* measurements of STS impacts to create a reference micro-debris environment. With this version of ORDEM, the process was expanded to account for the individual directionality of each STS window and radiator surface, and account for the altitude by STS mission. There is statistical confidence in the results at STS-mission altitudes for both MD and HD populations, which extrapolate to higher altitudes where there are no *in-situ* data. The micro-debris environment is dynamic, and while the ODPO continues to gather data from returned surfaces as available, the Shuttle no longer flies and equivalent returned surfaces are unlikely to be available soon. The best path forward is to plan for future instruments and experiments specifically designed for sampling the small-particle environment at higher altitudes (700 km and 1000 km) to study the sources and production mechanisms of micro-debris.

7   ACKNOWLEDGEMENTS

The authors are grateful to Dr. Phillip Anz-Meador for his expertise regarding *in-situ* micro-debris datasets and damage equations, and Debra Shoots for editorial assistance.

REFERENCES

1. Matney, M. An Overview of NASA's Orbital Debris Environment Model, Paper AAS 10-014, *Advances in the Astronautical Sciences, Vol. 137* (33rd AAS Rocky Mountain Guidance and Control Conference, Feb. 5-10, 2010, Breckenridge, CO.).

2. Hyde, J. Christiansen, E., and Lear, D. "Shuttle MMOD Impact Database." *Procedia Engineering*, Vol. 103, pp. 246-253, 2015.

3. Christiansen, E., Bernhard, R., and Hartsough, N. "Orbiter Meteoroid/Orbital Debris Impacts: STS-50 (6/92) through STS-86 (10/97)." JSC-28033 (August 1998).

4. Johnson, N.L. and McKnight, D.S. *Artificial Space Debris*, Orbit Book Company, Malabar, Florida, 1991.

5. Liou, J.-C., Anz-Meador, P.D., Hall, D.T., Krisko, P.H., Opiela, J.N. "LEGEND - a LEO-to-GEO environment debris model." *JSC-29711*, pp. 12-17, 2001.

6. Johnson, N.L., Krisko, P.H., Liou, J.-C., Anz-Meador, P., "NASA's New Breakup Model of EVOLVE 4.0," *Adv. Space Res.*, Vol. 28, No. 9, pp. 1377-1384, 2001.

7. Bjorkman, M.D., "Calculating the Presented Area Using BUMPER (MARK files)," memo to J.L. Hyde, ESCG-3400-11-008, September 2, 2011

8. Press, W.H., Teukolsky S.A., Vetterling, W.T., Flannery, B.P. *Numerical Recipes in Fortran 77*, Vol. 1, 2$\underline{nd}$ ed., Cambridge University Press, pp. 684-688, 1992.

9. Efron, B. & Tibshirani, R. J. *An Introduction to the Bootstrap*. London: Chapman & Hall/CRC, 1993.